Superconducting Transition Temperatures of Semiconducting $SrTiO_3$

C. S. KOONCE* AND MARVIN L. COHEN†
Department of Physics, University of California, Berkeley, California
AND
J. F. SCHOOLEY,‡ W. R. HOSLER,§ AND E. R. PFEIFFER
National Bureau of Standards, Washington, D. C.

(Received 5 July 1967)

The superconducting transition temperature T_c of $SrTiO_3$ has been measured for specimens having electron carrier concentrations n_c from 6.9×10^{18} to 5.5×10^{20} cm^{-3}. The curve exhibits a maximum in T_c for n_c near 9×10^{19} cm^{-3}. The transition temperature has also been calculated using one adjustable parameter ξ, the intervalley deformation potential, in addition to the known normal-state properties of $SrTiO_3$. A good fit to the experimental curve is obtained.

I. INTRODUCTION

FOLLOWING the application of the theory of superconductivity to the case of degenerate semiconductors and semimetals,[1] superconductivity was observed in the semiconducting compounds GeTe,[2] $SrTiO_3$,[3] and SnTe.[4] A brief discussion of the variation of the superconducting transition temperature T_c with electronic carrier density n_c for $SrTiO_3$ has been presented.[5] In that paper we pointed out that the curve of T_c versus n_c for $SrTiO_3$ contains a maximum value of T_c, although a rough application of the simple BCS expression[6] $T_c\approx\Theta_D \exp\{-1/[N(0)V]\}$ would predict a monatonic dependence of $\ln T_c$ on $(n_c)^{1/3}$ through the relation[7] $N(0)\sim n_c^{1/3}$. We also mentioned that the observed dependence of T_c on n_c could be explained qualitatively through the proper inclusion of screening of intervalley and intravalley interactions. We now have found the transition temperature at a larger number of concentrations in order to fix the curve T_c versus n_c more accurately, and, in addition, we have performed quantitative calculations which show that the experimental curve can be fitted quite closely using the measured properties of the system in the normal state and both intervalley and intravalley interactions.

Strontium titanate has been found to have a superconducting transition temperature greater than 0.05°K for electron concentrations in the conduction band between 8.5×10^{18} and 3.0×10^{20} cm^{-3}. This is the widest range of charge carrier concentrations over which any superconductor has been shown to be superconducting. In addition, these concentrations represent the lowest concentrations at which superconductivity has been observed.[8]

Because superconductivity occurs at such low carrier concentrations, we may assume a parabolic behavior of the conduction band near the Fermi surface which will be near the minima of the conduction band, and use the normal-state properties of the material to calculate the superconducting properties. The values for the normal-state properties used, along with references to the experiments by which they were measured, are given in Table I.

Since the complete curve of superconducting transition temperature as a function of carrier concentrations has been obtained, we can use the wealth of information contained in this curve to test our knowledge of the normal-state properties of $SrTiO_3$, and also to test the theory of superconductivity. Since the deformation potential for intervalley processes is not known for $SrTiO_3$, a value for it will be taken which gives a superconducting transition temperature near the experimental transition temperature at a given electronic concentration. The same value of the deformation potential will then be used to calculate the transition temperature at all concentrations. All other physical properties entering into the calculations will be taken within the experimental uncertainty in their measurement in the normal state. Since the transition temperature increases, reaches a maximum, and then decreases with increasing concentration, a one-parameter fit to the curve is quite demanding on the many normal-state parameters. Any substantial variation in the

* Present address: National Bureau of Standards, Washington, D.C. Supported in part by the National Science Foundation.
† A. P. Sloan Foundation Fellow. Supported in part by the National Science Foundation.
‡ Supported in part by the Advanced Research Projects Agency.
§ Supported in part by the National Aeronautics and Space Agency.

[1] M. L. Cohen, Phys. Rev. **134**, A511 (1964).
[2] R. A. Hein, J. W. Gibson, R. Mazelsky, R. C. Miller, and J. K. Hulm, Phys. Rev. Letters **12**, 320 (1964).
[3] J. F. Schooley, W. R. Hosler, and M. L. Cohen, Phys. Rev. Letters **12**, 474 (1964).
[4] R. A. Hein, J. W. Gibson, R. S. Allgaier, B. B. Houston, Jr., R. Mazelsky, and R. C. Miller, in *Proceedings of the Ninth International Conference on Low Temperature Physics*, edited by J. G. Daunt, D. V. Edwards, F. J. Milford, and M. Yaqub (Plenum Press, Inc., New York, 1965), p. 604.
[5] J. F. Schooley, W. R. Hosler, E. Ambler, J. G. Becker, M. L. Cohen, and C. S. Koonce, Phys. Rev. Letters **14**, 305 (1965).
[6] J. Bardeen, L. N. Cooper, and R. Schrieffer, Phys. Rev. **108**, 1175 (1957).
[7] See for example, Charles Kittel, *Introduction to Solid State Physics* (John Wiley & Sons, Inc., New York, 1956), 2nd ed., p. 250.
[8] Addition of a few percent $BaTiO_3$ reduces the minimum carrier concentration for superconductivity by more than an order of magnitude thus increasing the superconducting range even further. See J. F. Schooley, H. P. R. Frederikse, W. R. Hosler, and E. R. Pfeiffer, Phys. Rev. **159**, 301 (1967).

TABLE I. Parameters used in transition temperature calculations.

Property	Symbol	Value	References
Renormalized effective mass	m^*	$2.5\,m_0$	17, 26, 27
Band effective mass	$m_b{}^*$	$2.0\,m_0$	
Number of valleys in conduction band	ν	3.	19, 21
Total renormalization	Z^0	1.66–1.75	
Electronic contribution to normalization	$Z_C{}^0$	1.3	
Width of conduction band	$\mathcal{E}_{max}$	0.125 eV	21
High-frequency dielectric function at small wave vector	$\epsilon_\infty{}^{ra}$	5.2	a
High-frequency dielectric function for intervalley processes	$\epsilon_\infty{}^{er}$	2.0	15
Wave-vector difference between minima of conduction band	q_0	1.1395×10^8 cm^{-1}	12, 19, 21
Volume of unit cell	$\mathcal{V}_a$	5.927×10^{-23} cm^3	12
Mass in unit cell	M	3.0686×10^{-22} g	
Frequency of intervalley phonon	ω_{er}	1.2×10^{13} cps or 0.0497 eV	25
Damping of intervalley phonon mode	γ_0	0.015 eV	25
Effective charge parameters	Z_1, Z_2, Z_3	0.0584 eV, 0.00805 eV, 0.0238 eV	16
Damping of intervalley phonon modes	$\gamma_1, \gamma_2, \gamma_3$	0.0544 eV, 0.000855 eV, 0.00298 eV	16
Transverse optic phonon frequencies	ω_2, ω_3	0.0214 eV, 0.0675 eV	16
Lowest transverse optic phonon frequency	ω_1	$0.00129+0.0585\ q/q_0$	25, 28
Degeneracy of intervalley phonon mode	α	1	
Intervalley deformation potential	ξ	15.0 eV	

[a] W. G. Spitzer, R. C. Miller, D. A. Kleinman, and L. E. Howarth, Phys. Rev. **126**, 1710 (1962).

values of the normal-state parameters leads in general to a quite different curve of transition temperature as a function of carrier concentration. In addition, the fitting requires both intervalley and intravalley processes, and neither intravalley nor intervalley processes alone can account for the shape of the curve.

II. EXPERIMENTAL

A. Samples

The samples were cut to the desired size from single-crystal boules of pure strontium titanate (except for the specimens "Nb") and ground on all faces with #600 carborundum abrasive. In order to introduce the desired carrier concentration, they were treated by one of several methods at temperatures ranging from 800 to 1400°K and for times ranging from 2 to 90 h. Samples labeled HR were heated in flowing H_2 gas and cooled to room temperature under He gas. Samples labeled TiR were sealed in evacuated quartz capsules with small known amounts of Ti metal, which acts as an oxygen getter. This technique produced somewhat greater reductions with lower temperatures. Samples labeled Nb were obtained from boules grown with appropriate amounts of Nb_2O_5 powder added to the $SrTiO_3$ powder. They were grown by the Verneulli process but were largely polycrystalline. All Nb-doped samples were oxidized under O_2 gas at 700°K to 800°K for 10 h or longer.

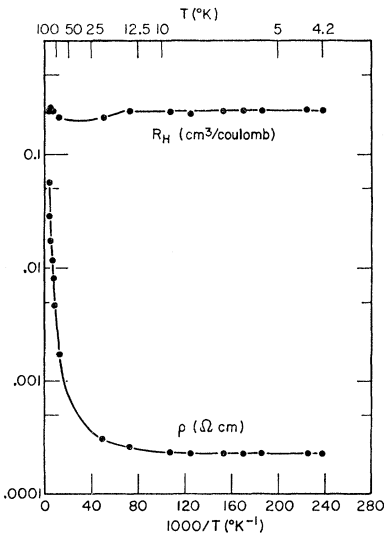

FIG. 1. Resistivity and Hall coefficient as a function of $1/T$ for sample HR6.

The Hall and normal conductivity measurements were made using the standard dc techniques. Contact arrangements were such that the Hall emf could be measured at several places along the sample to check for homogeniety in reduction or doping. Figure 1 shows a plot of $\log R_H$ and of $\log\rho$ versus $1/T$ for sample HR6 which is typical data for all samples. Both R_H and ρ remain nearly invariant with T from 10°K down to 1°K. Because of contacting difficulties and resulting noise, n_c values derived from R_H measurements have an accuracy of $\pm10\%$.

In repetitive superconductivity and Hall effect measurements, it was discovered that in certain specimens an apparent diminution of carriers occurred which seemed to be a function of the handling process before measurement. For this reason, most of the data illustrated in Fig. 2 were taken on the slab-shaped speci-

TABLE II. Properties of $SrTiO_3$ specimens.

Specimen	n_c (4.2°K) (cm^{-3})	ρ (4.2°K) (Ω cm)	μ (4.2°K) (cm^2/V sec)	Measured T_c (°K)	Calculated T_c (°K)
H*R*5	6.9×10^{18}	3.8×10^{-4}	2440		<0.07
H*R*52 slab	7.6×10^{18}	2.7×10^{-4}	3120	<0.06	0.07
	(7.6×10^{18})			(0.05)[a]	
Ti*R*2*b*	7.8×10^{18}	3.6×10^{-4}	2280	<0.07	
Ti*R*10 slab	8.5×10^{18}	3.4×10^{-4}	2210	0.06–0.07	
H*R*51 slab	9.4×10^{18}	4.2×10^{-4}	1620	0.085	0.07
H*R*22	1.0×10^{19}	2.8×10^{-4}	2280	<0.05	
H*R*28 slab	1.3×10^{19}	2.4×10^{-4}	2050	0.12	0.09
Nb8 slab	1.3×10^{19}	9.0×10^{-5}	5470	0.09	
H*R*27*c* slab	1.4×10^{19}	2.9×10^{-4}	1580	0.057	{0.10}[b] {0.08}
Ti*R*11 slab	1.5×10^{19}	3.2×10^{-4}	1330	0.07	
H*R*70 slab	1.66×10^{19}	3.3×10^{-4}	1170	0.127	0.10
Nb9 slab	1.89×10^{19}	7.5×10^{-5}	4510	0.183	
H*R*6 sph	(2.5×10^{19})[d]	(2.3×10^{-4})	(1110)	0.146	0.1496
H*R*6 slab	2.5×10^{19}	2.3×10^{-4}	1110	0.166	0.1477
H*R*72 slab	2.7×10^{19}	2.6×10^{-4}	912	{0.213}[c] {0.204}	0.15
H*R*3	3.1×10^{19}	4.0×10^{-4}	516	0.166	0.17
Ti*R*19 slab	4.9×10^{19}	2.6×10^{-4}	504	0.273	{0.25}[b] {0.24}
H*R*33 stress	(6.3×10^{19})[d]	(2.8×10^{-4})	(364)	0.278	
H*R*33 slab	6.3×10^{19}	2.8×10^{-4}	364	0.273	0.26
H*R*57	6.7×10^{19}	2.3×10^{-4}	415	0.275	
	(7.2×10^{19})			(0.290)[a]	0.26
H*R*24 sph	(1.0×10^{20})[d]	(2.8×10^{-4})	(280)	0.268	0.30
H*R*61 slab	1.1×10^{20}	2.6×10^{-4}	224	{0.280}[c] {0.283}	0.30
Ti*R*13 slab	1.2×10^{20}	2.4×10^{-4}	222	0.285	0.26
Nb10	1.5×10^{20}	6.1×10^{-5}	699	0.41	0.21
H*R*73 slab	1.66×10^{20}	2.2×10^{-4}	175	0.198	
H*R*74 slab	1.95×10^{20}	2.3×10^{-4}	143	0.120	0.15
Ti*R*2*a* slab	2.1×10^{20}	2.6×10^{-4}	117	0.295	0.12
H*R*69 slab	3.0×10^{20}	2.1×10^{-4}	102	0.06	0.04
	(4.0×10^{20})			(0.030)[a]	0.01
HC*R*2	5.5×10^{20}	1.7×10^{-4}	68	<0.05	0.002
	(5.5×10^{20})			(0.020)[a]	

[a] Transition temperatures assumed for purposes of the calculation.
[b] Double value indicates the range of purely computational uncertainty in the numerical calculation.
[c] Values found experimentally in two separate experiments.
[d] Normal-state properties measured on companion samples.

mens on which Hall and resistivity measurements had been made and which thus required no further special handling.

Table II contains a summary of normal-state and superconductivity data for the specimens discussed in this paper. Note that the mobility μ of the Nb-doped samples is 2 to 3 times larger than that of H*R*- or Ti*R*-reduced specimens for a given carrier concentration, in spite of the fact that the Nb-doped samples were polycrystalline. The degeneracy temperature for even the most lightly reduced sample is near 3°K, assuming a "density-of-states" mass $m_d^*=5m_0$.[9] The mobility also becomes constant with temperature at low temperatures which, assuming impurity scattering, suggests complete degeneracy.

B. T_c Measurements and Results

T_c Measurements

The temperature dependence of the magnetic susceptibility of each specimen was observed from about 0.05°K through T_c, using a mutual inductance apparatus operating at 270 Hz.

A schematic drawing of the low-temperature portion of the apparatus is shown in Fig. 3. For ease of handling,

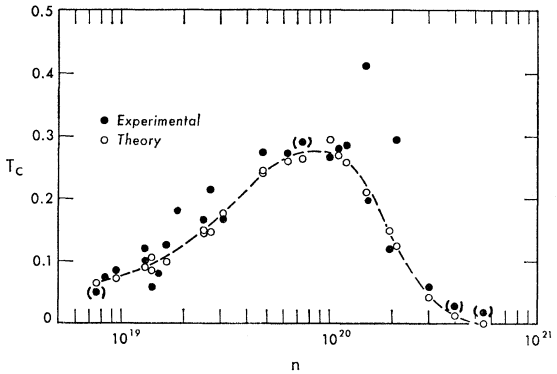

FIG. 2. Transition temperature as a function of carrier concentration. The plain solid circles represent experimental data. The bracketed solid circles are fictitious data used as input in the transition temperature calculation. The open circles show the results of the calculation, and the smooth dashed curve was drawn for illustrative purposes.

[9] H. P. R. Frederikse, W. R. Hosler, and W. R. Thurber, J. Phys. Soc. Japan Suppl. **21**, 32 (1966).

the apparatus was made top loading, so that specimens could be changed without raising the Dewar temperature above 4.2°K. The general cryogenic technique was similar to that described recently elsewhere,[8,10] with magnetic cooling pills L_1 and L_2 mounted so as to be thermally isolated from the pumped He^4 bath B at 1°K when He^3 exchange gas is removed from the vacuum jacket V. After adiabatic demagnetization, pill L_1 acts as a thermal reservoir at $T\approx 0.14$°K, and pill L_2 acts as a thermal reservoir for the thermometer pill T, an oriented single-crystal sphere of cerous magnesium nitrate (CMN), and for the specimen S. The mutual inductance pair P is composed of a 10:1:length: diameter primary coil and magnetically opposing 2100-turn secondary coils magnetically isolated by a factor of about 2500:1 from pill L_2.

The CMN thermometer sphere and the specimen were joined to the cooling wires C by daubs of vacuum stopcock grease, so that it was conceivable that substantial thermal gradients might exist between them. In order to measure this gradient, we placed a second CMN sphere at S during one experiment, and we compared the temperatures at S and T at nine temperatures between 0.06 and 0.6°K. The temperatures in each case were derived from extrapolations of the usual Curie-Law calibration curves of susceptibility versus temperature of pumped He^4 (using the T_{58} He^4 vapor-pressure–temperature relation) from 2 to 1°K. We found that the temperatures at S and at T so obtained agreed within 3 mdeg over the whole range of temperature measured, indicating quite good thermal equilibrium. We also found that equilibration times varied from $\approx$10 min at 0.06°K to $<$3 min at 0.12°K for the paramagnetic salt. One might expect faster thermal response from $SrTiO_3$ specimens as a consequence of their reduced heat capacity, so that one can safely regard thermal equilibration to be determined by the response of the paramagnetic thermometer T.

The susceptibility measurements were made in dc magnetic fields of less than 0.020 Oe and in ac measuring fields of a few millioersted. After adiabatic demagnetization of the system, a capacitor was discharged through H, a 1000-Ω Evanohm heater wire wrapped on the specimen. Use of this technique momentarily warmed the specimen to $T>T_c$ in order to expel trapped flux before the initial susceptibility measurements were made.

We found that the susceptibility was quite sensitive to the ac field amplitude near T_c. To avoid errors in this region, we restricted H_{ac} to about 1 mOe.

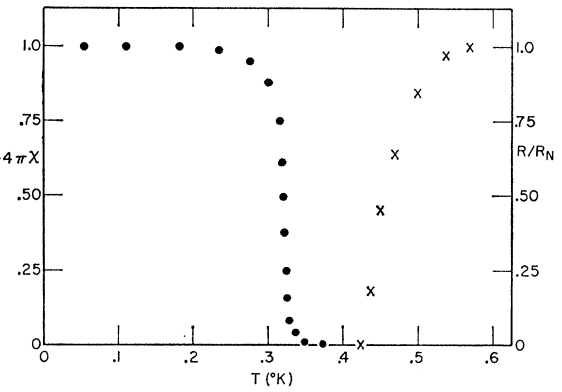

FIG. 4. Temperature dependence of the magnetic susceptibility and resistivity for sample HR24 slab.

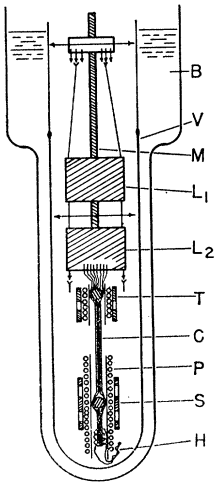

FIG. 3. Schematic drawing of low-temperature portion of mutual-inductance apparatus.

T_c Results

A typical curve of ac susceptibility versus temperature is shown in Fig. 4. For illustrative purposes, the reduced resistance as measured in the same experiment by the four-lead method is included. One can see in Fig. 4 that the superconducting transition curve is rounded on both the low-temperature and the high-temperature side, and that the specimen shows no resistance until yet a higher temperature is reached. Thus the assignment of a single T_c value, as in Table II and Fig. 2, is to some extent arbitrary. However, we have defined "T_c" for the purposes of this paper as the extrapolation to zero susceptibility of the steepest slope of the susceptibility curve. The following considerations entered into this choice: (1) Experiments with single-crystal $SrTiO_3$ specimens of various shapes, dimensions, and carrier concentrations have indicated that, as expected,[3] the zero-temperature superconducting penetration depth $\lambda(0)$ attains values greater than 10 μ in $SrTiO_3$.[11] Penetration depths of this magnitude produce a noticeable rounding off of the susceptibility curve below T_c in specimens of the dimensions studied in this work, so that the T_c as defined above is essentially that determined by considering penetration depth effects. (2) The extrapolation to zero of $H_{c1}(T)$, which has been measured for some of the specimens, and the observation of the superconducting heat capacity anomaly[10] produce values of T_c in good agreement with the

[10] E. Ambler, J. H. Colwell, W. R. Hosler, and J. F. Schooley, Phys. Rev. 148, 280 (1966).

[11] J. F. Schooley and W. R. Thurber, J. Phys. Soc. Japan Suppl. 21, 639 (1966).

present definition. (3) Preliminary measurements indicate that T_c is very sensitive to strain, so that strains arising either from specimen handling or from the small phase transitions which are seen in $SrTiO_3$ [12] can be expected to produce the magnetic and electrical effects shown in Fig. 4 above the bulk superconducting transition temperature.

Table II gives the results of over thirty experiments of the type discussed above. In two cases, specimens were rerun to check on reproducibility of the experimental apparatus. The differences in T_c in the two reruns amounted to 5 and 1%. In two other cases, different specimens cut from the same preparation were run. In these cases, T_c differed by 1 and 15%, the latter being specimen H*R*6, in which a change in n_c is suspected (see Sec. II. A). We estimate that exclusive of such changes in n_c, the errors in T_c and n_c are ± 5 and $\pm 10\%$, respectively.

III. THEORETICAL

We will now describe the methods used in the computation of the transition temperature in terms of the normal-state properties. After doing this, we will discuss the normal-state properties of $SrTiO_3$ that were used to calculate the superconducting properties.

The gap equation solved was

$$D(\mathcal{E}_k) = -Z(\mathcal{E}_k)^{-1} \int_{-\mathcal{E}_F}^{\mathcal{E}_{max}-\mathcal{E}_F} \frac{D(\mathcal{E}_{k'})}{E(\mathcal{E}_{k'})} K(c, \delta) \times \tanh\left(\frac{E(\mathcal{E}_{k'})}{2k_B T}\right) d\mathcal{E}_{k'}, \quad (1)$$

which, except for the renormalization $Z(\mathcal{E}_k)$ and the limits of integration, has been given previously by one of the authors.[1] $E(\mathcal{E}_k) = (\mathcal{E}_k^2 + \Delta_k^2)^{1/2}$ is the quasiparticle energy, $D(\mathcal{E}_k) = (k/k_F)\Delta_k$, $D(\mathcal{E}_{k'}) = (k'/k_F)\Delta_{k'}$, $c = k/k_F$, $\delta = \hbar\omega/\mathcal{E}_F = (\mathcal{E}_{k'} - \mathcal{E}_k)/\mathcal{E}_F$, and Δ_k is the energy gap. $\mathcal{E}_{max}$ is a maximum energy determined from the band structure of the material and is of the order of the energy width of the band. Since the effective-mass approximation is used in the calculation of $K(c, \delta)$ and the effective-mass approximation is not valid for energies near the maximum bandwidth, $\mathcal{E}_{max}$ is expected to be less than the average width of the band.

The kernel $K(c, \delta)$ is given by

$$K(c, \delta) = K^{ra}(c, \delta) + K_C{}^{er}(c, \delta) + K_{ph}{}^{er}(c, \delta), \quad (2)$$

where $K^{ra}(c, \delta)$ arises from intravalley interactions (both Coulomb and phonon), $K_C{}^{er}(c, \delta)$ arises from intervalley Coulomb interactions, and $K_{ph}{}^{er}(c, \delta)$ arises from the intervalley interaction between electrons through phonons. We find that each of these kernels makes an appreciable contribution to the total kernel and agreement between the calculated and experimental T_c versus n_c curve can only be obtained if all three contributions are included. This is in contrast to some recent calculations done in the high-carrier density limit,[13] indicating that only intravalley interactions may be responsible for superconductivity in $SrTiO_3$.

We will consider each contribution to the total kernel and discuss it in more detail. The kernels can be obtained from the interactions using Eq. (II.11) and Eq. (II.12) of Ref. 1. The intravalley kernel is given by

$$K^{ra}(c, \delta) = \frac{m_b{}^* e^2}{2\pi k_F \hbar^2 (\delta + c^2)^{1/2}} \times \int_{1/2|c-(\delta+c^2)^{1/2}|}^{1/2|c+(\delta+c^2)^{1/2}|} \frac{\epsilon_1{}^{ra}(\beta, \delta)}{\epsilon_1{}^{ra}(\beta, \delta)^2 + \epsilon_2{}^{ra}(\beta, \delta)^2} \frac{d\beta}{\beta}. \quad (3)$$

Here $m_b{}^*$ is the effective mass of a single electron in the conduction band when the ions are held rigid. We will call this the band mass. When renormalization and vertex corrections are included, $m_b{}^*$ in Eq. (3) will be multiplied by a vertex function and divided by $[1 + (d\chi/dE)]$, where χ is the Hartree-Fock energy. We will, however, absorb these modifications into our definition of $m_b{}^*$. In Eq. (3), $\beta = q/2k_F$, k_F is the Fermi wave vector, and the subscripts 1 and 2 on the intravalley dielectric function ϵ^{ra} refer to the real and imaginary parts, respectively. The intravalley dielectric function includes all processes, both Coulomb and phonon, which screen an electron. The total electron-electron interaction used in obtaining Eq. (3) is then

$$V^{ra}(q, \omega) = 4\pi e^2/\Omega q^2 \epsilon^{ra}(q, \omega), \quad (4)$$

where Ω is the volume of the crystal.

The real part of this interaction was taken as an approximation so that the kernel is taken to be real. $\epsilon^{ra}(q, \omega)$ can be written as a sum of electron and phonon polarizabilities as long as the interaction is not too strong. This addition of polarizabilities has been discussed for the case of a degenerate polar semiconductor.[14] The screening by electrons can be further broken down into screening by electrons in the valence band and screening by electrons in the conduction band. For electrons in the valence band, it has been shown[15] that, for frequencies much less than the gap frequency [which, for $SrTiO_3$, is 3.4 eV and is much larger than $\mathcal{E}_{max}$ appearing in Eq. (1)], their contribution to the dielectric function, which arises from interband transitions, approaches a constant value as the momentum transfer $\hbar q$ approaches zero, contrary to what would be expected from a free-electron model of the valence band. Reference 15 gives the dielectric constant $\epsilon_\infty(q)$ arising from interband transitions as a function of q over the entire Brillouin zone for a model band structure. We have used the notation $\epsilon_\infty(q)$ since, for frequencies much higher than all phonon frequencies and much higher than the plasma frequency of the elec-

[12] F. W. Lytle, J. Appl. Phys. **35**, 2212 (1964).

[13] J. Appel, Phys. Rev. Letters **17**, 1045 (1966).

[14] B. B. Varga, Phys. Rev. **137**, A1896 (1965).

[15] D. R. Penn, Phys. Rev. **128**, 2093 (1962).

trons in the conduction band, yet smaller than the gap energy over Planck's constant, the only contribution to the dielectric function arises from interband transitions, and is given by $\epsilon_\infty(q)$.

Because the Fermi surface of the free electrons in the conduction band takes up a small part of the Brillouin zone, we are interested primarily in two small regions of momentum space, near $q=0$ and near $q=q_0$. In these regions, $\epsilon_\infty(q)$ can be approximated by two constant values $\epsilon_\infty^{\rm ra}$ for intravalley transitions and $\epsilon_\infty^{\rm er}$ for intervalley transitions.

We note the limits of the integral in Eq. (3) run from $(2k_F)^{-1}\,|\,k-k'\,|$ to $(2k_F)^{-1}\,|\,k+k'\,|$ rather than from 0 to $2k_F$, as we would have if the energies of interest were much less than the Fermi energy, that is, $\delta\ll 1$. For strontium titanate, the highest concentration at which superconductivity was found was $n_c=3.0\times10^{20}$. Using three equivalent minima in the conduction band and the measured effective mass [not including renormalization (see Table I)], the Fermi energy was calculated to be 0.0314 eV. The ratio of the two strongest intervalley phonon energies to the Fermi energy at this highest concentration were 1.7 and 2.7. The ratio for the intervalley phonon of interest was 1.6. Therefore, the high-density approximation $\mathcal{E}_F\gg\hbar\omega_{\rm ph}$ is not valid over any range of concentrations studied, and the correct limits on the integrals must be maintained.

As Eq. (4) implies, the electrons in the conduction band can be treated as plane waves. If we approximate the wave function of an electron in a given valley by $\Omega^{-1/2}\exp[i(\mathbf{k}-\mathbf{k}_0)\cdot\mathbf{x}]$, a plane wave with wave vector referred to the minimum of the valley $\mathbf{k}_0$, and use a random-phase dielectric constant, we obtain a dielectric constant for a material with ν valleys which is similar to the one-valley plane-wave dielectric constant first obtained by Lindhard. We have

$$\epsilon_{\rm el}^{\rm ra}(\beta,\delta)_1=\epsilon_\infty^{\rm ra}+\frac{\nu 3\pi e^2 n_\nu\hbar^2}{32m^*\mathcal{E}_F^2\beta^3}\left\{[1-(\beta+\delta/4\beta)^2]\ln\left|\frac{1+\beta+(\delta/4\beta)}{1-\beta-(\delta/4\beta)}\right|\right.$$
$$\left.+[1-(\beta-\delta/4\beta)^2]\ln\left|\frac{1+\beta-(\delta/4\beta)}{1-\beta+(\delta/4\beta)}\right|+4\beta\right\};\quad(5)$$

$$\epsilon_{\rm el}^{\rm ra}(\beta,\delta)_2=-(\nu 3\pi^2e^2n_\nu\hbar^2/32m^*\mathcal{E}_F^2\beta^3)\times\delta,\quad\text{when }\beta<1\text{ and }\delta<|\,4\beta^2-4\beta\,|$$
$$\times[1-(\beta-\delta/4\beta)^2],\quad\text{when }|\,4\beta^2-4\beta\,|<\delta<|\,4\beta^2+4\beta\,|$$
$$\times 0,\quad\text{when }\delta>|\,4\beta^2+4\beta\,|$$
$$\times 0,\quad\text{when }\beta>1\text{ and }\delta<|\,4\beta^2-4\beta\,|,\quad(6)$$

where n_ν is the number of carriers in one valley, m^* is the effective mass including renormalization effects, and $\epsilon_{\rm el}^{\rm ra}(\beta,\delta)_1$ is the real part of the dielectric constant arising from screening by all electrons of intravalley processes, which we call $\epsilon_{\rm el}^{\rm ra}(\beta,\delta)$. $\epsilon_{\rm el}^{\rm ra}(\beta,\delta)_2$ is the imaginary part of $\epsilon_{\rm el}^{\rm ra}(\beta,\delta)$. A corresponding form for the dielectric function valid for the screening of intervalley processes will be given later.

In the case of $SrTiO_3$, the phonon contribution to the total dielectric function has been obtained near $q=0$ by infrared reflection measurements.[16] The polarizability of the phonon modes takes the form

$$\alpha_{\rm ph}(\omega)=\sum_{i=1}^{3}\frac{4\pi Z_i^2}{\omega_i^2-\omega^2+i\gamma_i\omega},\quad(7)$$

where the Z_i are the effective charges of the transverse modes ω_i. The γ_i are the damping of the ith mode and the sum over i goes over the three optically active modes of $SrTiO_3$. For q near zero, which is important for calculating the intravalley kernel, Eq. (7) should be a good approximation.

We note that for $q=0$ the acoustic phonons make no contribution to the dielectric function. For the small wave vectors of interest the contribution from acoustic phonons to intravalley processes will be smaller than the contribution from optic modes. We therefore will neglect the contribution of acoustic modes.

The total dielectric function can be obtained by adding the polarizabilities of the electrons in the conduction band, the electrons in the valence band, and the polarizability arising from the displacement of the ions. Since Eq. (5) already contains the polarizability of the valence-band and conduction-band electrons, we only need to add the ionic polarizability to this to obtain the total dielectric function;

$$\epsilon^{\rm ra}(q,\omega)=\epsilon_{\rm el}^{\rm ra}(q,\omega)+\alpha_{\rm ph}(\omega)=\epsilon_{\rm el}^{\rm ra}(q,\omega)+\sum_{i=1}^{3}\frac{4\pi Z_i^2}{\omega_i^2-\omega^2+i\omega\gamma_i}.\quad(8)$$

The total intravalley interaction given in Eq. (4) can be separated easily into a Coulomb interaction screened only by electronic processes and a Bardeen-Pines interaction between electrons through the phonon field screened by electronic processes. Inserting Eq. (8)

[16] A. S. Barker, Jr., Phys. Rev. 145, 391 (1966).

into Eq. (4), we have

$$V(q,\omega)=\frac{4\pi e^2}{\Omega q^2[\epsilon_{\rm el}{}^{\rm ra}(q,\omega)+\sum_i 4\pi Z_i{}^2/(\omega_i{}^2-\omega^2+i\omega\gamma_i)]}$$

$$=\frac{4\pi e^2}{\Omega q^2}\left\{[\epsilon_{\rm el}{}^{\rm ra}(q,\omega)]^{-1}-\sum_i\frac{4\pi Z_i{}^2/(\omega_i{}^2-\omega^2+i\omega\gamma_i)}{\epsilon_{\rm el}{}^{\rm ra}(q,\omega)[\epsilon_{\rm el}{}^{\rm ra}(q,\omega)+\sum_j 4\pi Z_j{}^2/(\omega_j{}^2-\omega^2+i\omega\gamma_j)]}\right\}, \quad (9)$$

or

$$V(q,\omega)=\frac{4\pi e^2}{\Omega q^2\epsilon_{\rm el}{}^{\rm ra}(q,\omega)}-\sum_i\frac{A_i(q,\omega)}{\tilde{\Omega}_i(q,\omega)^2-\omega^2+i\omega\gamma_i}, \quad (10)$$

where the strength of the ith mode is given by

$$A_i(q,\omega)=\left[\frac{4\pi e^2}{\Omega q^2\epsilon_{\rm el}{}^{\rm ra}(q,\omega)}\right]\left[\frac{4\pi Z_i{}^2}{\epsilon_{\rm el}{}^{\rm ra}(q,\omega)}\right], \quad (11)$$

and the ith renormalized longitudinal optic phonon frequency is given by the condition $\tilde{\Omega}_i{}^2(q,\omega)=\omega^2-i\omega\gamma_i$, where

$$\tilde{\Omega}_i{}^2(q,\omega)=\omega_i{}^2+\sum_j\frac{[4\pi Z_j{}^2/\epsilon_{\rm el}{}^{\rm ra}(q,\omega)](\omega_i{}^2-\omega^2+i\omega\gamma_i)}{\omega_j{}^2-\omega^2+i\omega\gamma_j}. \quad (12)$$

We note that Eq. (10) is not exactly in the Bardeen-Pines form, since $\tilde{\Omega}_i(q,\omega)$ depends on the frequency ω, and the longitudinal modes of the system occur when the denominator of Eq. (10) vanishes. In general, the denominator of Eq. (10) does not give a simple pole as does the Bardeen-Pines form [$\tilde{\Omega}_i{}^2(q,\omega)$ independent of ω]. These differences between the second term of Eq. (10) and the simple Bardeen-Pines form, although they are most important at small wave vector, do introduce modifications into the kernel and into the transition temperature as a function of n_c.[17]

The above discussion serves to emphasize the basic differences between superconductivity as it exists in metals and as it exists in degenerate semiconductors such as $SrTiO_3$. Although the density of states is comparable to that of a metal ($\gamma=1.60$ mJ deg^{-2} mole^{-1} when $n_c=1.4\times10^{20}$),[10] the carrier concentration n_c is much smaller than for a typical metal and the effective mass is larger. This means that the Fermi energy is no longer much larger than the phonon energies as is the case for metals, and also that electronic screening will be more important. These considerations must be taken into account in the calculation of the superconducting transition temperature.

Since the actual form of the intravalley interaction is known, that is, the known dielectric function Eq. (8) can be inserted into Eq. (4) and the interaction computed, the actual interaction was used in computing the kernel. This is, of course, an approximation to the Éliashberg form for the kernel.[18] To obtain the Éliashberg form for the kernel, we would have to make approximations for the phonon spectral weight function in the kernel (which would vary with concentration n_c). This process could introduce errors as large as would the approximation of the Éliashberg kernel by the kernel obtained from the normal-state electron-electron interaction. For this reason, the actual interaction, Eq. (4), was used in the calculation of the intravalley kernel $K^{\rm ra}(c,\delta)$.

The Coulomb contribution to the intervalley kernel is given by

$$K_C{}^{\rm er}(c,\delta)=\frac{(\nu-1)m_b{}^*e^2k_F}{\pi q_0{}^2\hbar^2(\delta+c^2)^{1/2}}\times\int_{1/2|c-(\delta+c^2)_1{}^{1/2}|}^{1/2|c+(\delta+c^2)^{1/2}|}\frac{\epsilon^{\rm er}(\beta_0,\beta,\delta)_1}{[\epsilon^{\rm er}(\beta_0,\beta,\delta)_1]^2+[\epsilon^{\rm er}(\beta_0,\beta,\delta)_2]^2}\beta d\beta, \quad (13)$$

where $\beta_0=q_0/2k_F$, and ν is the number of equivalent minima in the conduction band, separated from each other by the wave vector q_0. The wave-vector separation between electrons in different valleys is taken to be approximately equal to q_0. The interaction used in calculating $K_C{}^{\rm er}(c,\delta)$ was taken to be

$$V^{\rm er}(q,\omega)=\frac{4\pi e^2}{\Omega q_0{}^2\epsilon^{\rm er}(q_0,q,\omega)}, \quad (14)$$

where the screening, which is due only to electrons since the phonon contributions to the interaction between electrons is included in $K_{\rm ph}{}^{\rm er}(c,\delta)$, is approximated by

$$\epsilon^{\rm er}(\beta_0,\beta,\delta)=\epsilon_\infty{}^{\rm er}+\tfrac{2}{3}(\beta^2/\beta_0{}^2)[\epsilon_{\rm el}{}^{\rm ra}(\beta,\delta)-\epsilon_\infty{}^{\rm ra}]. \quad (15)$$

In obtaining Eq. (15), the electrons were taken to be plane waves centered in momentum space about the three equivalent valleys. The factor of $\frac{2}{3}$ arises because for a given wave vector only $\frac{2}{3}$ of the valleys are connected by the wave vector. The factor $\beta^2/\beta_0{}^2=q^2/q_0{}^2$ arises from the reduction of the bare Coulomb interaction occurring in the random-phase approximation to the dielectric function.

[17] M. L. Cohen and C. S. Koonce, J. Phys. Soc. Japan Suppl. **21**, 633 (1966). See also M. L. Cohen, in Superconductivity, edited by R. D. Parks (to be published).

[18] G. M. Éliashberg, Zh. Eksperim. i Teor. Fiz. **38**, 966 (1960) [English transl.: Soviet Phys.—JETP **11**, 696 (1960)].

The intervalley phonon interaction is given by

$$K_{\mathrm{ph}}^{\mathrm{er}}(c,\delta)=-\frac{(\nu-1)m_b^*k_F(\epsilon_\infty^{\mathrm{er}})^2q_0^2\alpha\xi^2}{2\pi^2(M/v_a)(\delta+c^2)^{1/2}\omega_{\mathrm{er}}^2}\times\left[\frac{1-(\delta/\delta_{\mathrm{er}})^2}{[1-(\delta/\delta_{\mathrm{er}})^2]^2+(\delta\delta_0/\delta_{\mathrm{er}}^2)^2}\right]\times\int_{(1/2)|c-(\delta+c^2)^{1/2}|}^{(1/2)|c+(\delta+c^2)^{1/2}|}\frac{\epsilon^{\mathrm{er}}(\beta_0,\beta,\delta)_1^2-\epsilon^{\mathrm{er}}(\beta_0,\beta_1\delta)_2^2}{[\epsilon^{\mathrm{er}}(\beta_0,\beta,\delta)_1^2+\epsilon^{\mathrm{er}}(\beta_0,\beta,\delta)_2^2]^2}\beta d\beta, \tag{16}$$

where M is the ionic mass, v_a the volume of a unit cell, and $\delta_0=\gamma_0/\mathcal{E}_F$. Here γ_0, the damping of the intervalley phonon mode, is included to approximate the effects of the dispersion of the phonon mode over the range of wave vectors in the integration as well as the decay of quasiparticles by phonon emission. $\delta_{\mathrm{er}}=\hbar\omega_{\mathrm{er}}/\mathcal{E}_F$, where ω_{er} is the frequency of the intervalley phonon allowed by symmetry. α is the degeneracy of this phonon mode and ξ is the intervalley deformation potential.

Equation (16) is obtained by using a screened Bardeen-Pines interaction between electrons through exchange of a phonon for the one phonon mode allowed by crystal symmetry and time reversal:

$$V_{\mathrm{ph}}^{\mathrm{er}}(q,\omega)=\frac{-2\hbar\omega_{(q)}\,|\,M(q)\,|^2}{[\epsilon^{\mathrm{er}}(q_0,q,\omega)/\epsilon_\infty^{\mathrm{er}}]^2[\omega_{(q)}^2-\omega^2]}. \tag{17}$$

Since the Fermi wave vectors of the electrons in each valley are small compared to the wave-vector difference between minima in the band q_0, the intervalley dielectric function is approximated by Eq. (15), the matrix element $M(q)$ is approximated by $M(q_0)$, and the effect of the dispersion of the phonon mode over the range of q used in the calculation of the kernel $K_{\mathrm{ph}}^{\mathrm{er}}(c,\delta)$ is roughly included by inserting a damping term into Eq. (17).

We then have

$$V_{\mathrm{ph}}^{\mathrm{er}}(q,\omega)=-\frac{2\hbar\omega_{\mathrm{er}}\,|\,M(q_0)\,|^2}{[\epsilon^{\mathrm{er}}(q_0,q,\omega)/\epsilon_\infty^{\mathrm{er}}]^2(\omega_{\mathrm{er}}^2-\omega^2+i\gamma_0\omega)}, \tag{18}$$

where $|\,M(q_0)\,|^2=\alpha\hbar^2q_0^2\xi^2/2(M/v_a)\Omega\hbar\omega_{\mathrm{er}}$, and where ω_{er} is the frequency of the intervalley phonon of wave vector q_0. The intervalley phonon kernel Eq. (16) is then obtained from the intervalley phonon interaction Eq. (18) using Eq. (II.12) of Ref. 1. In general, the interaction through the phonon field given by Eq. (18) would contain a sum over phonon modes. For the case of $SrTiO_3$, however, only one phonon mode is allowed by symmetry to couple electrons near two different minima in the first Brillouin zone.

The calculations of Kahn and Leyendecker[19] indicate that the minima of the conduction band lie at the points **X** of the cubic Brillouin zone of $SrTiO_3$ and that the electrons have symmetry $\mathbf{X}_3$ of the group O_h, where the notation used is that of Bouckaert, Smoluchowski, and Wigner.[20] The positions of the minima have been verified by magnetoresistance measurements[21] and Shubnikov–deHaas effect.[22] The number of equivalent minima in the conduction band ν is therefore 3. This is supported by the large values of the "density-of-states effective mass" (see discussion later). The origin of coordinates in real space is chosen by Kahn and Leyendecker to be the titanium atom. This is convenient since the electrons transforming as $\mathbf{X}_3$ are made from titanium $3d$ orbitals in the tight-binding approximation.

The wave vector q_0 connecting two equivalent minima at **X** lies at the edge of the Brillouin zone which is labeled **M**. Using the results of Lax and Hopfield[23] and Lax,[24] we can find the requirements on a given phonon mode of wave vector q_0 imposed by symmetry and time reversal which must be met if the matrix element $M(q_0)$ is to be nonzero.

The matrix element $M(q_0)$ describes a phonon transforming according to the group **M** between electronic states transforming like $\mathbf{X}_3$ in two different equivalent directions. From symmetry requirements, we have that only phonons of symmetry $\mathbf{M}_3$ and $\mathbf{M}_4$ (using BSW notation) are allowed. Time reversal rules out $\mathbf{M}_4$, so that only $\mathbf{M}_3$ is allowed.

The phonon spectrum of $SrTiO_3$ has been measured in the [100] direction and calculated in other directions by Cowley[25] who uses the strontium atom as the origin of coordinates and a somewhat different notation from that of BSW. From the compatibility relation given in Ref. 25, one can determine that the phonon transforming as $\mathbf{M}_3$ using the titanium atom as the origin of coordinates transform according to $\mathbf{M}_1$ using Cowley's conventions.

Although other intervalley phonon modes are not strictly forbidden for q_0 not at M, the low concentrations of electrons over which superconductivity occurs indicates that the contribution to the kernel $K_{\mathrm{ph}}^{\mathrm{er}}(c,\delta)$ of phonon modes forbidden at q_0 will be much less than the contribution of phonons allowed by symmetry and time reversal at q_0. Only the one allowed phonon mode was therefore used in the intervalley phonon interaction.

Having obtained expressions for the kernel in Eqs. (2), (3), (13), and (16), we proceed to calculate the superconducting transition temperature from Eq. (1).

The renormalization $Z(\mathcal{E}_k)$ was approximated by a constant, which we will call Z^0, over the width of the

[19] A. H. Kahn and A. J. Leyendecker, Phys. Rev. **135**, A1321 (1964).

[20] L. P. Bouckaert, R. Smoluchowski, and E. Wigner, Phys. Rev. **50**, 58 (1936). This reference will be referred to as BSW.

[21] H. P. R. Frederikse, W. R. Hosler, and W. R. Thurber, Phys. Rev. **143**, 648 (1966).

[22] H. P. R. Frederikse, W. R. Thurber, W. R. Hosler, J. Babiskin, and P. Siebenmann, Phys. Rev. **158**, 775 (1967).

[23] M. Lax and J. J. Hopfield, Phys. Rev. **124**, 115 (1961).

[24] M. Lax, *Report of the Exeter International Conference on the Physics of Semiconductors* (The Institute of Physics and The Physical Society, London, 1962), p. 395.

[25] R. A. Cowley, Phys. Rev. **134**, A981 (1964).

band. Actual calculations of $Z(\mathcal{E}_k)$ indicate that this is a good approximation (within 20%) for all $\mathcal{E}_k$ and an even better approximation to the average $Z(\mathcal{E}_k)$. The constant Z^0 was obtained from a two-square-well model. Although this is crude by the standards of the method of solving the integral equations, the errors introduced into the calculated transition temperature by using a two-square-well approximation in the calculation of Z^0 are much smaller than the errors introduced by using a two-square-well model to calculate the transition temperature from Eq. (1).

We use the relation

$$Z^0 = Z_C^0 + (Z_{ph}^0 - 1), \tag{19}$$

where Z_C^0 and Z_{ph}^0 are the Coulomb and phonon contributions to the renormalization, respectively. Z_{ph}^0 was determined from the two-square-well approximation as

$$Z_{ph}^0 = 1 + (\log 1.14\hbar\omega_{er}/k_0T_c)^{-1} + \frac{2K_C(0)}{1+2K_C(0)\log(\mathcal{E}_{max}/\hbar\omega_{er})}. \tag{20}$$

$K_C(0)$ is the total Coulomb kernel, given by the sum of $K_C^{ra}(0)$ and $K_C^{er}(0)$. $K_C^{ra}(0)$ is easily obtained from the first term of Eq. (10), and $K_C^{er}(0)$ from Eq. (13). The phonon frequency in Eq. (20) is taken to be the intervalley phonon frequency.

The Coulomb contribution to the renormalization Z_C^0 is estimated for a typical concentration and held constant over the range of concentrations studied.

A feature of this method of calculating the renormalization is that it uses an estimate of the transition temperature (usually the experimental value) to calculate Z_{ph}^0. A high estimated T_c leads to a large value of Z_{ph}^0, while a low estimated T_c leads to Z_{ph}^0 nearer 1. The value of Z_{ph}^0 obtained in this way is then used in Eqs. (19) and (1) to obtain a theoretical T_c. Since Z^0 appears in the denominator of Eq. (1), a large Z^0 lowers the theoretical T_c more than a smaller value of Z^0.

If the experimental value of the transition temperature were too large, for example, the value that we would obtain for Z^0 would also be too large. This value of Z^0 would lead to a theoretiecal T_c which would be too small. Also, if the theoretical phonon kernel in Eq. (16) were in error, the method that we use to obtain Z_{ph}^0 would not affect the corresponding error in the transition temperature. This is in contrast to the method of calculating Z_{ph}^0 from first principles, in which case errors in the phonon kernel tend to be reduced by corresponding errors in Z_{ph}^0 for purposes of calculating transition temperatures.

We have calculated T_c for both H*R*6 spherical and for H*R*6 slab. (See Table II.) The difference in the theoretical values of T_c arises entirely from the different experimental transition temperatures obtained for these samples. Also, to illustrate the range of uncertainty arising from computational approximations involved in the calculations, we show two theoretical transition temperatures for samples H*R*27*c* and Ti*R*19. These approximations will be discussed later.

We will now briefly discuss the normal-state properties used in the evaluation of the kernels in Eqs. (3), (13), and (16).

The conduction-band structure of $SrTiO_3$ has been approximated by parabolas centered at the minima of the conduction band and extending upward in energy to a maximum energy $\mathcal{E}_{max}$. The partially renormalized density of states to be used in the integral equation can then be described by an isotropic effective mass independent of energy m_b^*. The effective mass near the Fermi energy is then the same over the entire range of concentrations studied. This approximation is probably the most serious in the calculation of the transition temperature over a wide range of concentrations, since a change in the effective mass near the Fermi energy at different concentrations would lead to changes in T_c at some concentrations relative to T_c at other concentrations. It is expected that the effective mass varies with increasing energy above the band minima, but sufficient experimental data were not available to determine this precisely, and theoretical calculations of the effective mass do not have high enough accuracy at this time to warrant their use. The band effective mass m_b^* was therefore determined at one point near the peak of the T_c versus n_c curve ($n_c = 1.4\times10^{20}$) and taken to be constant over the range of concentrations studied.

The mass occurring in the dielectric function m^* includes the effects of renormalization and is related to the "density-of-states effective mass" determined from measurements of the density of states for a degenerate semiconductor with ν equivalent valleys by the relation $\nu^{2/3}m^* = m_d^*$, where m_d^* is the "density-of-states effective mass." The "density-of-states effective mass" has been determined through a measurement of the electronic contribution to the normal-state specific heat at low temperatures.[10] These measurements yield $\gamma = 1.60$ mJ deg^{-2} mole^{-1} for $n_c = 1.4\times10^{20}$, which gives m^* near $2.5m_0$. This value of m^* was used in the dielectric screening for all concentrations and, in addition, was used to estimate a value for m_b^*.

The effective mass can also be obtained from spin susceptibility measurements, but since the renormalization modifies the mass in a different way, this mass is expected to be less than m^*. The effective masses obtained from spin susceptibility measurements[26] are 2.45 and $2.38m_0$ for $n_c = 7.5\times10^{19}$ and 5.3×10^{20}, respectively. These measurements, made at 4.2°K, give effective masses slightly smaller than the specific-heat effective mass, and the effective mass at the Fermi energy apparently does not change rapidly with concentration.

[26] H. P. R. Frederikse and G. A. Candela, Phys. Rev. **147**, 583 (1966).

The effective mass has also been measured through measurements of transport properties[27]; however, these measurements have been carried out only at higher temperatures. At 78°K, these experiments yield m^* near $3.3m_0$.

The eccentricity of the ellipsoids which are the form of the Fermi surface in $SrTiO_3$ has been determined from magnetoresistance measurements.[21,22] The ratio of the longitudinal (parallel to the k_x direction if the minimum lies at the face of the Brillouin zone in the k_x direction) to the transverse (perpendicular to k_x) direction, m_l/m_t, is 4.0. The elliptical nature of the Fermi surfaces does affect the transition-temperature calculation through the fact that, for a given concentration, some electrons in different valleys are closer together in momentum space than they would lie if the valleys were spherical. This causes an increase in Coulomb repulsion and a more rapid screening of the interactions at high carrier concentrations, and hence a smaller T_c at large concentrations for elliptical rather than spherical valleys. For $m_l/m_t=4.0$, however, this effect is relatively unimportant and the curve of T_c versus n_c was fitted using spherical valleys about the minima of the conduction band.

The phonon contributions to the renormalization [Eq. (20)] was found to vary from 1.36 for $n_c=9.4\times10^{18}$ to 1.45 at $n_c=3.0\times10^{20}$, always increasing with increasing carrier concentration over the range of concentrations studied.

The kernels were cut off due to band-structure effects before the natural cutoff of the Coulomb kernels. The width of the conduction band $\mathcal{E}_{max}$ has been estimated to be 0.13 eV.[21] Due to our parabolic approximation, a smaller value of 0.125 eV was used in our calculation.

In the cubic Brillouin zone, the wave vector connecting different nonopposite faces lies at **M** and has magnitude $q_0=\sqrt{2}\pi/a_0$, whereas the lattice constant was determined from the x-ray measurements of Lytle[12] to be near 3.899×10^{-8} cm (assuming the crystal to be cubic near 1°K). This lattice constant was also used to find the volume of the unit cell $\mathcal{V}_a$.

As we mentioned previously, the effective charges, damping, and transverse optic (TO) phonon frequencies entering into the phonon polarizability [Eq. (7)] have been obtained near $q=0$ from infrared reflection measurements.[16] These measurements were made at 300 and 90°K. As the temperature is lowered below 90°K, the static dielectric constant increases rapidly, reaching a value near 22 500 at 0.3°K.[28] In accordance with the suggestion of Anderson[29] and Cochran,[30] the lowest transverse optic phonon frequency decreases with decreasing temperature, the phonon frequency being proportional to $\epsilon^{-1/2}$. Therefore, while all other intravalley parameters were approximated by the measured values at 90°K, the lowest TO phonon frequency at $q=0$ was adjusted to give the observed value of the static dielectric constant.

The marked decrease of the lowest TO phonon mode occurs only very near $q=0$, and the frequency of the mode varies appreciably over wave vectors of the order of k_F for typical electron concentration, as can be seen from the neutron-scattering measurements of Cowley.[25] The wave vector dependence of the lowest TO phonon mode must be considered, therefore. The approximation to its dispersion used is given in Table I.

After performing the integrals indicated in Eqs. (3), (13), and (16) numerically with the aid of a computer, the total kernel, Eq. (2), was obtained. Using the total kernel, the transition temperature was obtained from Eq. (1) using an extension of the square-well model proposed by Tolmachev[31] to many wells, again with the help of a computer.

From Table II, we see that two theoretical values for T_c were calculated for samples H*R*27*c* and Ti*R*19. These different values of T_c resulted from evaluating the wells at different energies and thus sampling the kernel at different energies. The different values of T_c give the approximate magnitude of the error in T_c arising from the use of a finite number of wells.

IV. DISCUSSION

Figure 2 and Table II give the transition temperatures obtained experimentally and theoretically as a function of carrier concentration n_c. The most noticeable deviation between the theoretical and experimental transition temperature is the large value for T_c of 0.41°K in sample Nb10 having a carrier concentration of 1.5×10^{20} cm^{-3}. A peak in this region was not found theoretically. The theoretical curve lies within the scatter of the experimental curve at all concentrations and at low concentrations shows a positive curvature (when plotted as a function of $\log n_c$) which is not apparent from the experimental points, but which is within the probable experimental uncertainty.

It should be noted that the transition temperatures were calculated for the normal-state parameters listed in Table I, which we believe to be well within the present experimental error in the determination of these quantities. If other values are chosen for the normal-state properties, in general, the fit of the experimental and theoretical points is not as good. In addition, we may have compensated, to some extent, for approximations in the calculation of the transition temperature by a choice of normal-state parameters different from their true values. For example, the assumption of a

[27] H. P. R. Frederikse, W. R. Thurber, and W. R. Hosler, Phys. Rev. **134**, A4421 (1964).
[28] Esturo Sawaguchi, Atsichi Kikuchi, and Yoichi Kodera, J. Phys. Soc. Japan **17**, 1666 (1962).
[29] P. W. Anderson, in *Fizika Dielektrikov*, edited by G. I. Skanavi (Akad. Nauk SSSR Fizicheskii Inst. Im. P. N. Lebedeva, Moscow, 1960).
[30] W. Cochran, Advan. Phys. **9**, 387 (1960).
[31] N. N. Bogoliubov, V. V. Tolmachev, and D. V. Shirkov, *New Method in the Theory of Superconductivity* (Consultants Bureau, New York, 1958).

constant mass m_b* may have caused an overestimation of the transition temperature at high concentrations which might be compensated in part by a underestimation of ϵ_∞^{er} and an overestimation of ξ. On the other hand, the plane-wave approximation for the electrons has caused the matrix elements normally appearing in Eqs. (4), (6), (14), and (15) to be equal to one. Both band-structure effects and renormalization would tend to reduce these matrix elements. This approximation caused the theoretical calculation of T_c at high carrier concentrations to be too small relative to those at lower concentrations, arising from the overestimation of Coulomb interactions and Coulomb screening. The error due to this approximation is, therefore, cancelled to some extent by the constant-mass approximation. The error due to the plane-wave approximation could, therefore, be compensated in part by an underestimation of ϵ_∞^{er}.

It was found, however, that it was quite difficult to obtain even a crude fit to the curve of transition temperature as a function of concentration using normal-state values noticeably different from those given in Table I. In general, the variation of one normal-state parameter would produce a change in the T_c versus n_c curve which could not be compensated by any choice of other normal-state properties within the bounds of experimental knowledge.

From the calculations of the transition temperature as a function of carrier concentration, we can state that the principal attractive interaction over most of the carrier concentration range studied is the intervalley phonon interaction. The inclusion of both intravalley and intervalley processes is necessary to fit the measured T_c versus n_c curve, the intravalley processes being relatively most important at the lowest concentrations studied. In addition, the normal-state properties are probably close to the values chosen in Table I, since large variations from the values in Table I produce T_c versus n_c curves which lie outside the limits of the experimentally determined curve.

PHYSICAL REVIEW VOLUME 163, NUMBER 2 10 NOVEMBER 1967

Quantum Theory of Superfluid Vortices. II. Type-II Superconductors*

ALEXANDER L. FETTER

Institute of Theoretical Physics, Department of Physics, Stanford University, Stanford, California

(Received 5 July 1967)

The London model of bulk type-II superconductors is used to derive the dynamical equations of quantized flux lines. These equations are rewritten in a Hamiltonian form, and the system is quantized by interpreting the conjugate variables as quantum-mechanical operators that obey the canonical commutation relations. Diagonalization of the Hamiltonian yields the exact dispersion relation for small-amplitude waves propagating with arbitrary wave vector in the vortex lattice. This formalism allows a straightforward calculation of the specific heat associated with thermally excited lattice vibrations and of the mean-square displacement of the vortex cores. Similar features are shown to occur in the mixed state of a thin superconducting film in a perpendicular magnetic field.

I. INTRODUCTION

THE mixed state of a bulk type-II superconductor is characterized by a regular array of quantized flux lines.[1] These lines lie parallel to the magnetic field **H** and consist of a core of radius ξ (the coherence length) surrounded by circulating supercurrents confined to a larger radius λ (the penetration depth). In an extreme type-II sample ($\lambda \gg \xi$) well below its upper critical field ($H \ll H_{c2}$), the mean distance b between flux lines is much larger than ξ. The core regions therefore occupy a negligible fraction of the total volume and may be replaced by singularities in the superfluid velocity field. This approximation represents the fundamental assumption of the London model[2–10]; it allows a simple description of the quantized flux lines as

* Research sponsored by the Air Force Office of Scientific Research Office of Aerospace Research, U.S. Air Force, under AFOSR Contract No. AF49(638)1389.

[1] A. A. Abrikosov, Zh. Eksperim. i Teor. Fiz. **32**, 1442 (1957) [English transl.: Soviet Phys.—JETP **5**, 1174 (1957)].

[2] F. London, *Superfluids* (Dover Publications, Inc., New York, 1961), Vol. I, Sec. B.

[3] J. Friedel, P. G. de Gennes, and J. Matricon, Appl. Phys. Letters **2**, 119 (1963).

[4] P. G. de Gennes and J. Matricon, Rev. Mod. Phys. **36**, 45 (1964).

[5] J. Matricon, Phys. Letters **9**, 289 (1964); J. Matricon, in *Proceedings of the Ninth International Conference on Low Temperature Physics, Columbus, Ohio, 1964* edited by J. G. Daunt, D. O. Edwards, F. J. Milford, and M. Yaqub (Plenum Press, Inc., New York, 1965), p. 544.

[6] P. G. de Gennes, *Superconductivity of Metals and Alloys* (W. A. Benjamin, Inc., New York, 1966), Chap. 3.

[7] B. B. Goodman, Phys. Letters **18**, 8 (1965); B. B. Goodman, Rept. Progr. Phys. **29**, 445 (1966).

[8] B. B. Goodman and J. Matricon, J. Phys. Radium **27**, Suppl. C3, 39 (1966).

[9] A. L. Fetter, P. C. Hohenberg, and P. Pincus, Phys. Rev. **147**, 140 (1966).

[10] A. L. Fetter and P. C. Hohenberg, in *Superconductivity*, edited by R. D. Parks (M. Dekker, Inc., New York, to be published).